processes

MDPI

Article

Tunable Electrical and Fatigue Performance of Carbon Nanotube-Embedded Bottlebrush Elastomers via Compositional Control

Abby Jackson and Yuncheng Du *

Department of Biomedical Engineering, University of Houston, Houston, TX 77004, USA; ajacks23@cougarnet.uh.edu
* Correspondence: ydu20@uh.edu

Abstract

Bottlebrush elastomers (BBEs) are promising for flexible and wearable electronics due to their mechanical resilience. Incorporating conductive nanofillers such as carbon nanotubes (CNTs) enables the tuning of their electrical properties. This work studies the electrical properties of CNT–bottlebrush elastomer composites by varying polydimethylsiloxane (PDMS)/crosslinker ratios and CNTs loadings. Building on established synthesis methods, this study investigates how compositional changes affect conductivity, sensitivity, and fatigue behavior. Our results show a composition-dependent trade-off between electrical and mechanical fatigue performance, offering insights into tailoring these composites to meet specific performance requirements in next-generation soft electronics.

Keywords: bottlebrush elastomers (BBEs); carbon nanotubes (CNTs); conductive composites; flexible electronics; conductivity; sensitivity; fatigue resistance

check for updates

Academic Editors: Yongchao Yu, Ming Xiao and Shutong Wang

Received: 9 October 2025
Revised: 4 November 2025
Accepted: 6 November 2025
Published: 7 November 2025

Citation: Jackson, A.; Du, Y. Tunable Electrical and Fatigue Performance of Carbon Nanotube-Embedded Bottlebrush Elastomers via Compositional Control. *Processes* **2025**, *13*, 3613. https://doi.org/10.3390/pr13113613

Copyright: © 2025 by the authors. Licensee MDPI, Basel, Switzerland. This article is an open access article distributed under the terms and conditions of the Creative Commons Attribution (CC BY) license (https://creativecommons.org/licenses/by/4.0/).

1. Introduction

Flexible and wearable electronics have gained growing interest for health monitoring, which creates a strong demand for soft, stretchable materials that maintain reliable electrical performance under mechanical deformation [1,2]. Among various promising materials, bottlebrush elastomers (BBEs) have recently received great attention due to their unique architectures, which include the densely grafted side chains along a linear backbone that can minimize polymer entanglements and offer exceptional softness [3]. Unlike other soft materials like hydrogels, BBEs are solvent-free, offering improved long-term stability for applications across diverse environments [4].

Polydimethylsiloxane (PDMS)-based BBEs are particularly promising for soft electronics, which combine biocompatibility, thermal and chemical stability, and ultra-low elastic moduli [5]. However, a key limitation of PDMS-based BBEs is their intrinsic electrical insulation [6]. To address this, conductive nanofillers, such as carbon nanotubes (CNTs) [7], graphene [8], metallic nanowires [9], or conductive polymers [10] have been incorporated into the BBEs matrices to create conductive hybrid composites [11]. Among these, CNTs are especially popular due to their superior electrical conductivity and mechanical resilience [12]. Early studies have reported the role of CNTs as multifunctional reinforcements that are capable of forming conductive networks even at low filler concentrations [13].

Recent research has focused on integrating CNTs into soft polymer matrices to develop conductive materials for strain sensing, motion tracking, and bioelectronic interfaces. Xu et al. reported ultrasoft CNT–bottlebrush composites that achieved satisfactory

conductivities of 2.68–13.78 S/m while maintaining an ultra-low Young's modulus of 2.98–10.65 kPa [11]. This work demonstrates the feasibility of balancing conductivity and elasticity to create a soft conductive elastomer. Similarly, Peng et al. emphasized the importance of filler alignment and percolation pathways for achieving stable electromechanical performance under deformation [14]. These studies highlight that CNTs not only affect conductivity but also influence viscoelastic behavior and fatigue response. Therefore, understanding how CNTs content and network morphology interact with matrix stiffness is essential for designing high-performance elastomers for wearable strain sensors and soft robotics where both sensitivity and durability are critical.

While the feasibility of CNTs/PDMS-BBEs composites has been demonstrated [11], most prior studies have focused on synthesis protocols, with limited systematic evaluation of how compositional parameters affect functional properties of the resulting materials. In particular, the effects of variables such as the PDMS-to-crosslinker molar ratio and CNTs' loading on conductivity, mechanical sensitivity, and fatigue resistance remain underexplored [15]. These properties are critical for engineering and tailoring soft composites for dynamic applications, where materials are often subjected to continuous deformation such as bending [16]. Furthermore, material selection frameworks such as the multi-criteria decision-making approach used by Bulut et al. ranked thermoplastic polymers for hybrid-vehicle battery packs [17]. The framework evaluates both performance and sustainability criteria to balance the engineering design. Similar approaches have been used to rank biobased polymers based on end-of-life pathways, for example, reuse and mechanical recycling, while also meeting functional performance criteria [18]. Although our present work focuses on mechanical and electrical functionalization, we adopt a comparable mindset by systematically varying composition and evaluating relationships between structure and functionality. Additionally, recent advances in BBEs synthesis, which include solvent-free formulations and organocatalytic polymerization, as well as the development of 3D printable bottlebrush elastomers, have further expanded the design space for functional materials [19]. However, significant challenges remain. Among them, the integration of electrical functionality into BBEs without compromising mechanical integrity is still a major materials design challenge [7,11].

This study addresses these challenges by embedding CNTs into PDMS-based BBEs to fabricate conductive composites. We systematically investigate how variations in material compositions affect the electromechanical and fatigue behavior of the resulting composites. Using a scalable, solvent-free synthesis approach, we collect data to demonstrate how a balance can be achieved between conductivity, sensitivity, and durability. Unlike conventional PDMS hydrosilylation that relies on Pt catalysts, we use a metal-free, AIBN-initiated radical hydrosilylation to eliminate catalyst residues while achieving elastomer curing [20]. Our findings show a composition-dependent trade-off in performance and provide a framework for tailoring the composites for the next generation of soft electronic devices and health monitoring.

2. Materials and Methods

2.1. Materials

Polydimethylsiloxane (PDMS; MCR-M11) was used as the base polymer for BBEs synthesis. MCR-M11, purchased from Gelest (Morrisville, PA, USA), has a molecular weight of 1000 g/mol and a density of 0.96 g/mol. Its terminal vinyl groups and low viscosity enable efficient crosslinking, which results in soft elastomers with tunable mechanical properties [21]. The crosslinker (DMS-R22) was also obtained from Gelest (Morrisville, PA, USA) and used to crosslink the PDMS via thermal initiation. DMS-R22 has a molecular weight of 10,000 g/mol and a density of 0.98 g/mol. The crosslinker

contains reactive Si-H bonds that form covalent links with the PDMS chains [22]. Moreover, thermal initiator 2-2′-Azobisisobutyronitrtile (AIBN) was purchased from Sigma-Aldrich (St. Louis, MO, USA). AIBN has a molecular weight of 164.21 g/mol and decomposes upon heating to generate nitrogen gas and free radicals, which further facilitate polymerization and promote synthesis [23].

Single-walled carbon nanotubes (SWCNTs) were purchased from Tuball (Leudelange, Luxembourg), which have diameters of about 1–2 nm and aspect ratios of up to 10,000. They were chosen over multi-walled CNTs in this work due to their superior structural flexibility, high surface area, electrical conductivity, and mechanical strength which collectively make them ideal for building conductive networks within elastomeric matrices [24].

Basic alumina (Sigma-Aldrich, St. Louis, MO, USA) and cotton were also used as purification materials to remove impurities from the PDMS and crosslinker. Alumina serves as a polar absorbent that can remove contaminants, while the cotton provides a physical filter. Additionally, ultra-high purity nitrogen gas was purchased from Matheson (Houston, TX, USA). The nitrogen gas was used to create an inert atmosphere during the thermal curing process, which prevents unwanted oxidation and premature degradation of the BBE/SWCNT composite. The soft-tipped four-point probe used for conductivity testing was purchased from Ossila (Sheffield, United Kingdom). Copper foil tape also used for conductivity testing was purchased from Amazon (Seattle, WA, USA). Copper tape (6.35 mm wide) was chosen due to its high electrical conductivity and ease of use without damaging the composite samples.

2.2. Synthesis of Bottlebrush Elastomers

2.2.1. Purification of PDMS and Crosslinker

Prior to synthesis, the PDMS and crosslinker (CL) were purified to remove impurities that could affect the crosslinking reaction. As illustrated in Supplementary Figure S2, a custom-made purification column was assembled. Specifically, a 10 mL syringe without the needle was packed with an approximately 3 mm layer of cotton at the bottom as the base, followed by 3 g of basic alumina powder.

The syringe was then placed above a 50 mL collection tube and stabilized using aluminum foil. PDMS and crosslinker were individually passed through the alumina column under gentle pressure and gravity. Approximately 10 mL of each material were purified using the column, which takes around 10 min. The process was repeated in batches until the required volume for BBE synthesis was obtained. The purified materials were then collected in airtight centrifuge tubes and stored in a 4 °C fridge to prevent degradation and contamination.

2.2.2. Synthesis of Bottlebrush Elastomers with Carbon Nanotubes

Conductive BBEs composites were synthesized by thermally curing PDMS and crosslinker mixtures with CNTs. The base elastomer mixture was prepared by mixing the PDMS and crosslinker at three molar ratios of 600:1, 800:1, and 1000:1. The molar ratios were calculated based on 10 mL of PDMS, and crosslinker volumes were adjusted accordingly. Following this, AIBN was added to the mixture at 2 mol% relative to the PDMS to initiate crosslinking under elevated temperatures around 80–85 °C. The precursor mixture (PDMS, crosslinker, and AIBN) was then vortexed for 8 min at 10,000 rpm using a high-speed vortex to ensure homogeneity and uniform distribution throughout the elastomeric mixture. Uniform mixing was confirmed visually.

The specific formulations of all composites, including PDMS/crosslinker ratios, CNT loadings, and initiator concentration are summarized in Supplementary Table S1. This

table provides a detailed overview of the experimental matrix used for composite synthesis and clarified the proportional relationship between components of each formulation.

Following this, CNTs were added to the precursor at different target weight percentages, i.e., 0.4, 0.6, or 0.8 wt.%. SWCNTs were weighed using a precision balance and gradually added into the vortexed precursor to avoid agglomeration. A serological pipette was used to add around 5 mL of the precursor to the weighing boat containing the CNTs and then it was transferred into a 25 mL Erlenmeyer flask with a small magnetic stir bar. This process was repeated until all the CNTs and precursor mixture were combined in the flask.

To prevent premature crosslinking and facilitate dispersion, the flask was placed in an ice bath, which was prepared by filling a 500 mL glass beaker with crushed ice up to 200 mL. The Erlenmeyer flask was placed inside the larger beaker so that no ice entered the flask. The mixture was stirred at 900 rpm for 90 min on a stir plate setting the temperature at 0 °C to prevent the ice melting, making sure the flask was kept on ice at all times. The stirring time was selected as 90 min to ensure sufficient deagglomeration and uniform distribution of SWCNTs throughout the elastomer matrix but not too long since this could damage the CNTs due to prolonged shear forces [25]. Proper CNT dispersion is critical for achieving conductive networks. Poor dispersion or excessive shear forces can cause breakage of the CNTs and reduce the electrical performance [26]. Stirring at moderate speed and low temperature helped us to avoid structural degradation of the CNTs and preserved their aspect ratio and conductivity.

After stirring, the composite mixture was transferred to a custom-made polytetrafluoroethylene (PTFE) mold using a serological pipette. PTFE was chosen as the mold material because it is chemically inert and has low surface energy which enables clean sample removal after curing. The filled mold was placed in a vacuum overnight (Yamato vacuum drying oven) at room temperature (around 22 °C) to degas the sample to remove any trapped air bubbles that were introduced during mixing and addition of the CNTs. This step is important to produce a defect-free composite that has consistent mechanical and electrical properties.

The samples were then cured in the same oven at 80 °C for approximately 12 h under continuous nitrogen purging. Nitrogen purging was used to maintain an inert atmosphere during curing and prevent oxidative degradation of the PDMS matrix and SWCNT network. The process results in a solid, uniformly crosslinked elastomeric composite with homogeneous distribution of CNTs.

In brief, the vinyl-terminated PDMS and hydride-functional crosslinker (DMS-R22) in this work occurs through a radical hydrosilylation process initiated by AIBN rather than the conventional use of a transition metal catalyst [27]. When heated to approximately 80–85 °C, AIBN decomposes to form free radicals that abstract hydrogen from Si-H bonds in the crosslinker, producing reactive silyl radicals. These silyl radicals then add across the vinyl groups on PDMS, forming Si-C linkages that connect the polymer chains and create a crosslinked elastomer network.

This mechanism eliminates the need for a metal catalyst which avoids residual platinum contamination and improves the purity of the material. This is important for wearable and bio-integrated reactions. The reaction proceeds efficiently under nitrogen to prevent oxygen inhibition and unwanted side reactions. The overall radical hydrosilylation pathway is summarized in Supplementary Figure S3 [20].

Although AIBN-initiated radical curing proceeds via a metal-free route, the resulting Si-C crosslinks are permanent, yielding a thermoset network rather than a thermoplastic one. This is consistent with other reports of PDMS-based hydrosilylation elastomers that do not exhibit melt reprocessing upon heating [21].

2.2.3. Sample Preparation

The cured BBE composites containing SWCNTs were carefully removed from the PTFE mold and cut into rectangular samples (e.g., size 20 mm × 30 mm) using a sharp razor blade. Conductivity testing was performed by using both a two-point method and a four-point probe approach. The thickness of each sample was measured using a digital caliper and recorded. All samples were separately stored at room temperature in sealed Petri dishes for subsequent testing and characterization.

2.3. Characterization Techniques

2.3.1. Morphology

The morphology and dispersion of the SWCNTs within the BBE matrix were characterized using scanning electron microscopy coupled with energy-dispersive X-ray spectroscopy (SEM-EDS). Cured elastomers samples were cut into small pieces and placed directly onto silicon wafers. Imaging and composition analysis was performed by using Axia-ChemiSEM equipment operating at an accelerating voltage of 15 kV under a high vacuum to examine the surface morphology and assess the dispersion of SWCNTs within the elastomer matrix. SEM images were also taken after fatigue testing to determine any surface morphology changes. EDS analysis was conducted to verify elemental composition and to confirm the presence and distribution of carbon nanotubes.

For EDS analysis, samples were mounted on silicon wafers to reduce carbon background signal and allow for more accurate elemental mapping of CNT distribution. Elemental quantification included carbon (C), oxygen (O), and silicon (Si). The results of synthesized samples with a PDMS/crosslinker molar ratio of 600:1 were chosen in this work for morphological demonstration. This formulation was selected because its relatively low crosslink density facilitates clear visualization of internal microstructures.

To directly characterize the morphology of SWCNTs, additional SEM imaging was conducted using a FEI DB235 focused ion beam at 15 kV. For this, approximately 0.5 mg of SWCNTs were dispersed in 5 mL of ethanol, vortexed for 3 min and drop-cast onto a silicon wafer using a pipette. Samples were air-dried at room temperature to allow complete ethanol evaporation before imaging.

2.3.2. Electrical Conductivity Testing

The electrical conductivity of synthesized composites was measured first using a four-point probe approach with a Keithley 2614B SourceMeter (Tektronik Inc., Beaverton, OR, USA). This approach minimizes contact resistance effects that may occur at the electrode interface and provides a higher accuracy for soft conductive materials such as BBEs [28].

Rectangular samples were cut to dimensions of 20 mm × 30 mm. The outer two probes supplied a constant current, while the inner two probes measured the corresponding voltage drop across the sample. The conductivity was calculation using Equation (1):

$$\sigma = \frac{L}{R\,A} \tag{1}$$

where σ is the conductivity (S/m), L is the distance between electrodes or probe spacing (m), R is the electrical resistance (Ω) obtained from V/I (voltage/current), and A is the cross-sectional area of the same (m^2). All measurements were performed at room temperature (~22 °C) and repeated five times for each composition to ensure reproducibility.

Additionally, conductivity tests were performed using a two-probe setup with copper-tape electrodes and the results are included in the Supplementary Figures S11–S13 for comparison with previous reports [11,29,30]. These measurements captured general conductivity trends as a function of CNT loading and crosslinking ratio; however, they were

likely affected by contact resistance and pressure effects at the electrode interface, especially during bending and compression tests. Therefore, four-point probe measurements were subsequently conducted under identical conditions in this work.

Similarly to the four-point test, copper tape electrodes were affixed to opposing ends of each testing sample for the two-point method. Resistance measurements were collected at room temperature using a Keithley 2614B Source Meter. The conductivity was then calculated from the resistance using Equation (1). For two-point probe testing the distance between the electrodes was measured as 17.3 mm.

Angle-dependent conductivity testing was conducted to evaluate anisotropic behavior. Samples were placed at various angles (varying from 0° to 90° with a 15° increment) using 3D printed wedges as shown in Supplementary Figure S4. The wedges were printed using Anycubic photon mono 4K with SyriaTech UV resin to ensure accuracy. Conductivity was measured at each angle. Of note, these angles were chosen since they provide a systematic and evenly spaced dataset so variation in conductivity can be evaluated. For each measurement, the sample was placed on the appropriate wedge for testing, and all measurements were repeated five times to ensure reproducibility. The average of five measurements was calculated and presented in the Results section. Additional visualization was performed by normalizing each value to its baseline conductivity for each sample. This normalization highlights the conductivity change and enables comparison across samples under different test conditions. These normalized data for both a two-point method and a four-point probe approach are shown in Supplementary Figures S11–S16.

2.3.3. Sensitivity Testing

The sensitivity of the resulting BBEs/CNTs composites to external mechanical pressure was evaluated using a layered paper method, which enabled gradual pressure increases to test materials performance. Samples were placed flat on a nonconductive surface, and layers of standard office paper cut into 15 mm × 15 mm squares and weighing 18.32 mg were incrementally stacked over the sample surface to provide a consistent pressure increment. The number of paper layers ranged from 0 to 10 to create pressure gradient.

Electrical resistance was measured after each additional layer using both four-point and two-point probe methods with a Keithley 2614B source meter. The sample was allowed to stabilize for ~10–15 s before resistance was recorded to account for any viscoelastic effects in the composites. Conductivity was calculated from resistance using the same methods as Section 2.3.2. Three repeated measurements were collected at each point to ensure more accurate and reliable results, with the average value and standard deviation calculated. No conversion from added mass to pressure was performed since the number of paper layers accounted for the increasing load. This method enabled an assessment of the relationship between the number of paper layers and conductivity to evaluate the material's potential for pressure-based sensing applications.

2.3.4. Fatigue Testing

The fatigue performance of the BBEs/CNTs composites was evaluated using manual cyclic bending tests to simulate repeated mechanical deformation and assess the stability of the conductive network. Each sample was manually bent to 90° and then released to return to its original configuration (Supplementary Figure S5). Bending was conducted at room temperature (around 22 °C) and repeated for different cycle counts of 50, 100, 150, 200, 300, 400, 500, 600, 700, 800, 900, and 1000 with resistance measured after each interval using both the two-point and four-point probe methods.

Each bend–release cycle was performed at an estimated rate of ~1 cycle every 2 s, with the sample held briefly (approximately 1 s) at the peak 90° bend before release. In this

work, it is important to note that, while the bending location on the sample was not fixed, bending was applied along different random positions on each sample surface across cycles to avoid localizing stress and to simulate real-world usage conditions such as wearable or flexible devices where stress is often distributed unpredictably. This approach allowed for a more general evaluation of durability across the full sample. It is acknowledged that manual bending introduces some variability in angle, rhythm, and strength; however, this was minimized by the same experimentalist and using a consistent bending rhythm. This manual approach was chosen for its simplicity and relevance to practical deformation scenarios in soft electronics as uncertainty commonly exists. Future studies may further explore automated bending equipment for more precise control, but current results provide a realistic assessment of the composite's fatigue behavior.

3. Results

3.1. Material Synthesis and Morphology

Figure 1a shows an SEM image with magnification of 10.1 kV to demonstrate the SWCNT networks. The image shows the individual tubular morphology of the CNTs, which contributes to their conductivity properties. Figure 1b–d show SEM images of the cured BBE/CNT composites with a PDMS/crosslinker molar ratio of 600:1 and CNT loadings of 0.4, 0.6, and 0.8 wt.%, respectively. At the lowest loading of 0.4 wt.%, Figure 1b, CNTs appear sparsely distributed, with several isolated bundles visible on the surface. Increasing the CNT concentration to 0.6 wt.% results in a denser and more continuous network as shown in Figure 1c, indicating improved interconnection between the carbon nanotubes. At 0.8 wt.% in Figure 1d, the CNTs create an almost fully percolated network, with locally entangled regions that suggests the onset of partial agglomeration. Overall, the change in distribution from 0.4 to 0.8 wt.% demonstrates an increase in CNT connectivity while maintaining a generally uniform dispersion, confirming that the mixing of the CNTs was effective within the BBE matrix.

To further evaluate elemental composition in composites, energy-dispersive X-ray spectroscopy (EDS) was conducted on BBEs samples with different CNTs loadings of 0.4 wt.%, 0.6 wt.%, and 0.8 wt.%. This analysis aims to quantitatively confirm the successful incorporation of CNTs into the BBE matrix and to analyze how increasing the CNTs content in the samples affects that relative atomic distribution of the elements carbon (C), oxygen (O), and silicon (Si). These three elements were chosen for quantification because carbon is a major component of both PDMS and the SWCNTs. This provides insight into the changes in composition due to CNT loading. Oxygen and silicon are native to the PDMS backbone, which help track compositional changes in polymer content with increasing CNT loading.

For characterization, samples of BBE/CNT composites were placed on silicon wafers. As seen in Figure 1e, EDS quantification revealed an increase in the carbon atomic percentage as the CNT wt.% increased. This confirms successful incorporation of CNTs into the bottlebrush elastomer matrix and is consistent with increased CNT content. The increase in carbon content suggests the CNTs are both physically embedded in the sample and well-distributed across material surface, which aligns with the morphological observations in Figure 1b–d, where the CNT network becomes denser and more continuous at higher loadings.

Additionally, oxygen levels remained stable for the samples ranging from 22.8% to 25.1%, indicating stable PDMS content. The fluctuations in oxygen might be introduced by surface oxidation due to exposure of the samples to air during handling. The silicon content, on the other hand, showed a decreasing trend with increased CNT loading. This is expected since an increased CNTs content displaces some of the PDMS, which is the main source of silicon. The decrease in silicon with the increase in carbon content emphasizes the inverse

relationship between PDMS content and CNT loading and the change in composition. It is also worth mentioning that although the use of silicon wafers may have slightly overestimated the absolute silicon content due to the background signal from the substrate, all samples were characterized under identical preparation and measurement conditions. Therefore, the observed trend of decreasing silicon content with increasing CNT loading remains valid for comparative purposes.

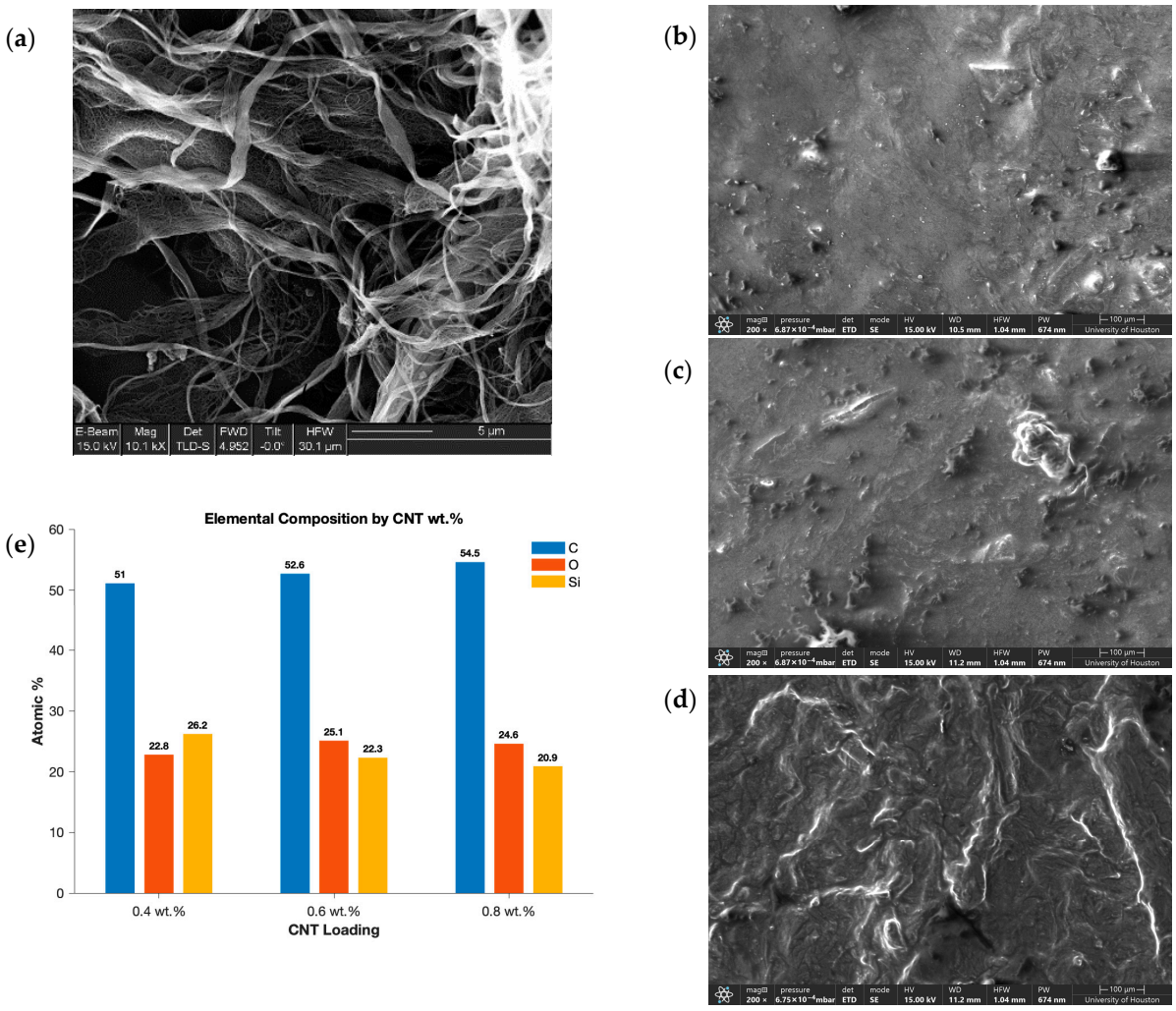


Figure 1. (**a**) SEM of single-walled carbon nanotubes (SWCNTs). (**b**–**d**) SEM-EDS of BBE/SWCNT composite 600:1, (**a**) 0.4 wt.%, (**b**) 0.6 wt.%, (**c**) 0.8 wt.% CNT. (**e**) Elemental composition of carbon (C), oxygen (O), and silicon (Si) for 600:1 sample with 0.4 wt.%, 0.6 wt.%, and 0.8 wt.% CNT.

Additionally, elemental carbon (C-K) count maps for the 0.4, 0.6, and 0.8 wt.% samples are provided in Supplementary Figure S6. These maps further confirm the uniform spatial distribution of carbon throughout the elastomer matrix across all loadings, with increasing pixel intensity corresponding to higher CNT concentrations. The consistent dispersion observed across all samples supports the quantitative EDS data and demonstrates effective incorporation of CNTs during synthesis.

3.2. Electrical Conductivity

Figure 2a shows the conductivity result of samples tested on a flat surface. As seen, for all formulations with different molar ratios between PDMS and crosslinker, conductivity increased as CNT loading increased from 0.4 to 0.8 wt.%. This trend is expected as a

higher CNT content can facilitate more interconnected conductive pathways throughout the elastomer matrix.

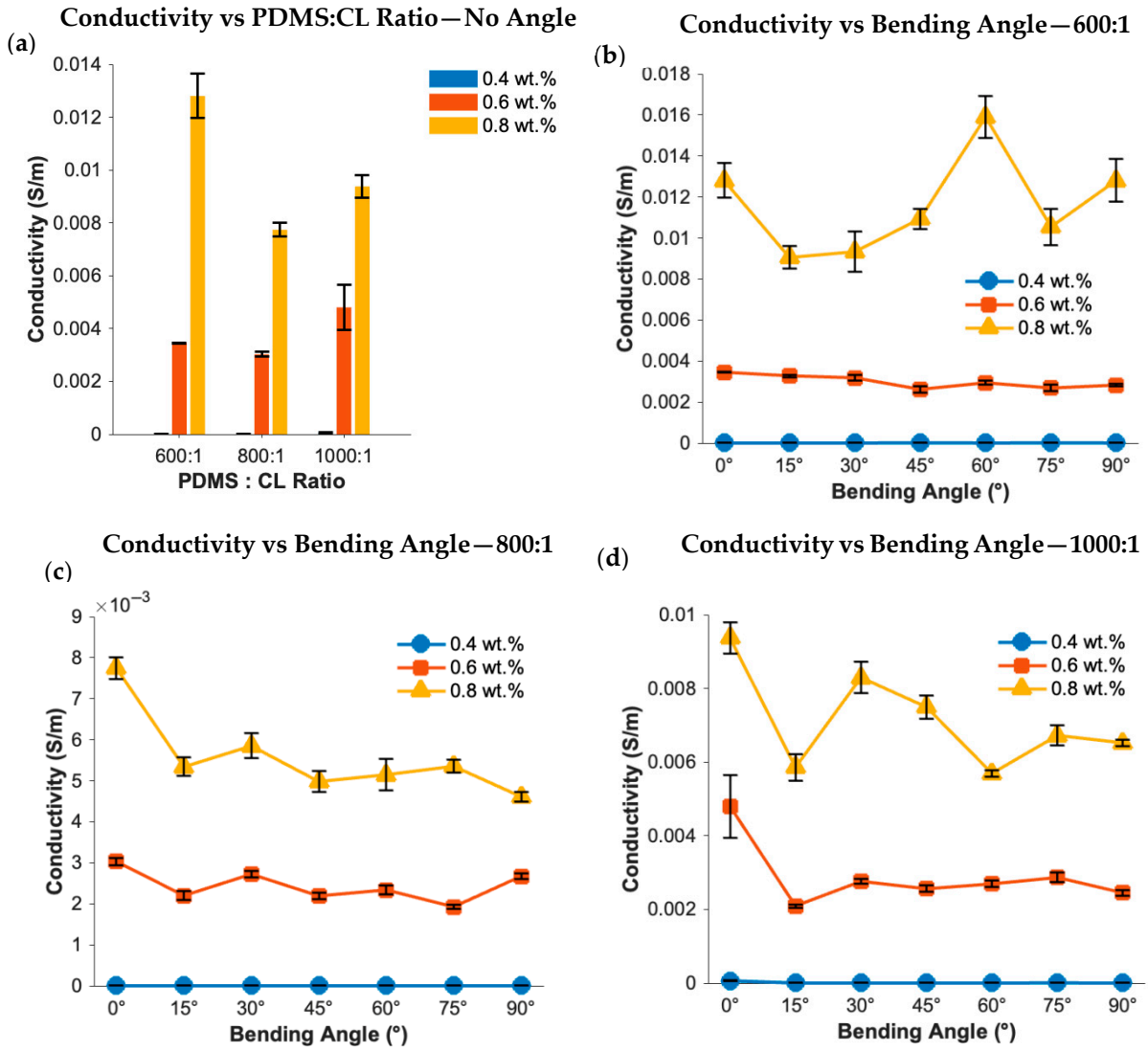


Figure 2. (**a**) Conductivity vs. PDMS/crosslinker (CL) ratio (600:1, 800:1, 1000:1) at 0.4, 0.6, and 0.8 CNT wt.%. (**b**–**d**) Conductivity of CNT/BBE composites as a function of bending angle (0–90°) for PDMS/CL ratios of 600:1, 800:1, and 1000:1, respectively, using the four-point probe testing approach.

For different molar ratios between PDMS and crosslinker with a 0.4 wt.% CNT loading, all formulations showed low conductivity (<0.002 S/m) for the four-point probe test. This suggests that at this concentration, the CNTs remain below the percolation threshold, resulting in insufficient conductive pathways similar to a prior report [31]. The limited interconnectivity at 0.4 wt.% suggests that CNTs are too sparsely distributed to form continuous networks.

For the 0.6 wt.% CNT loading, conductivity significantly improved across all samples with different molar ratios of the PDMS and crosslinker. For example, the samples with a molar ratio of 1000:1 showed the highest conductivity ~0.005 S/m, while samples with ratios of 600:1 and 800:1 reached about 0.003~0.004 S/m, respectively. These results suggest that the 1000:1 formulation likely supports better network formation at low to moderate CNT concentrations, possibly due to a more connected network that preserves conductive paths.

At 0.8 wt.% CNT loading, all the samples exhibited a significant increase in conductivity: 600:1 (0.013 S/m), 800:1 (0.007 S/m), and 1000:1 (0.009 S/m). Interestingly,

the 600:1 formulation resulted in the highest conductivity at 0.8 wt.% CNTs. This may be because the denser crosslinking network offers enhance structural stability and promotes a more uniform CNT dispersion. This suggests that above a critical CNT loading, the influence of crosslinking density may have diminished, and all systems can support robust percolated networks.

Overall, this data highlights the compositional interplay between CNT loading and crosslinking density. At lower CNT content, network stability may play a great role. However, once a threshold loading is surpassed (~0.8 wt.%), all samples achieve high conductivity, indicating effective percolation regardless of crosslinking ratio.

3.3. Angle-Dependent Conductivity

Figure 2b–d present the conductivity response of the CNT/BBE composites under bending for PDMS/CL ratios of 600:1, 800:1, and 1000:1. Overall, the conductivity trends reveal composition-dependent electromechanical stability, where both CNT loading and crosslinking density strongly affect how well conductive networks withstand deformation.

For the 600:1 formulation in Figure 2b, the 0.8 wt.% CNT composite showed the highest conductivity (~0.009–0.016 S/m) but also exhibited noticeable fluctuation across bending angles. This variation suggests that at high CNT loadings, while a dense percolation network ensures high conductivity, local agglomeration and microcrack formation during bending may intermittently disrupt contact between CNT clusters [32]. These transient resistive changes produce the observed conductivity oscillations. In contrast, the 0.6 wt.% sample showed lower but more stable conductivity values (~0.003 S/m) across all angles, suggesting that a moderately connected CNT network offers a better balance between electrical continuity and elastic compliance. At this intermediate loading, the CNTs are sufficiently interconnected to form a continuous conductive network, while still being sufficiently dispersed to allow the polymer matrix to deform without creating a high-stress concentration [33]. The conductivity of the 0.4 wt.% sample remained relatively low ($<2 \times 10^{-5}$ S/m) but still exhibited some variation, as shown more clearly in Supplementary Figure S8. This fluctuation likely arises from partial reformation and breakage of isolated conductive paths as the sample bends, typical of materials near the percolation threshold [34,35].

At the 800:1 ratio in Figure 2c, the same overall trend of conductivity was observed with the 0.8 wt.% sample, which exhibits the highest conductivity. The 0.8 wt.% sample showed a slight decrease in conductivity as bending increased while the 0.6 wt.% maintained a consistent conductivity around 0.0025 S/m with minimal drift. These results indicate that the softer matrix (from the reduced crosslinking density) accommodated deformation more evenly, minimizing strain that could disrupt conductive networks. However, the 0.4 wt.% samples again showed a low conductivity ($<1 \times 10^{-5}$ S/m) with small amplitude fluctuations in Supplementary Figure S8b likely caused by the isolated CNT clusters making and breaking contact under mechanical stress.

For the 1000:1 composite in Figure 2d, conductivity ranged from ~0.006 to 0.009 S/m for the 0.8 wt.% samples. The 0.8 wt.% sample again showed slightly greater variability compared to the 0.6 wt.% sample, which remained relatively flat apart from a drop at 15°. This sudden decrease is likely caused by localized strain of the conductive junctions. At low bending angles, tensile stress is concentrated near the surface where slight separation of CNT junctions can result in a loss of conductivity [33]. However, this still suggests that a moderate CNT content produces the most stable and resilient conductive network, as it minimized both filler aggregation and strain-induced detachments. The 0.4 wt.% samples also demonstrated low conductivities, with occasional spikes seen at intermediate angles in Supplementary Figure S8c, reflecting unstable behavior at low CNT loadings.

Overall, these results reveal a key trade-off. High CNT loading enhances absolute conductivity but introduces greater signal variability, while moderate CNT loading (0.6 wt.%) yields a more stable conductivity under repeatable deformation, which is consistent with previous findings [28]. Although the 0.4 wt.% samples were below the percolation threshold, they displayed transient conductive variations which highlights the sensitivity of these samples. This composition-dependent behavior highlights the importance of optimizing CNT content to balance conductivity and mechanical reliability in soft conductive composites.

3.4. Sensitivity Performance

Figure 3a–c present the sensitivity of the CNT/BBE composites to compressive loading, represented by the number of paper layers placed on top of these samples for PDMS/CL ratios of 600:1, 800:1, and 1000:1. Using the four-point probe approach, this test evaluated how conductivity changes with externally applied subtle pressure and provides insight into the materials potential for pressure-sensing applications.

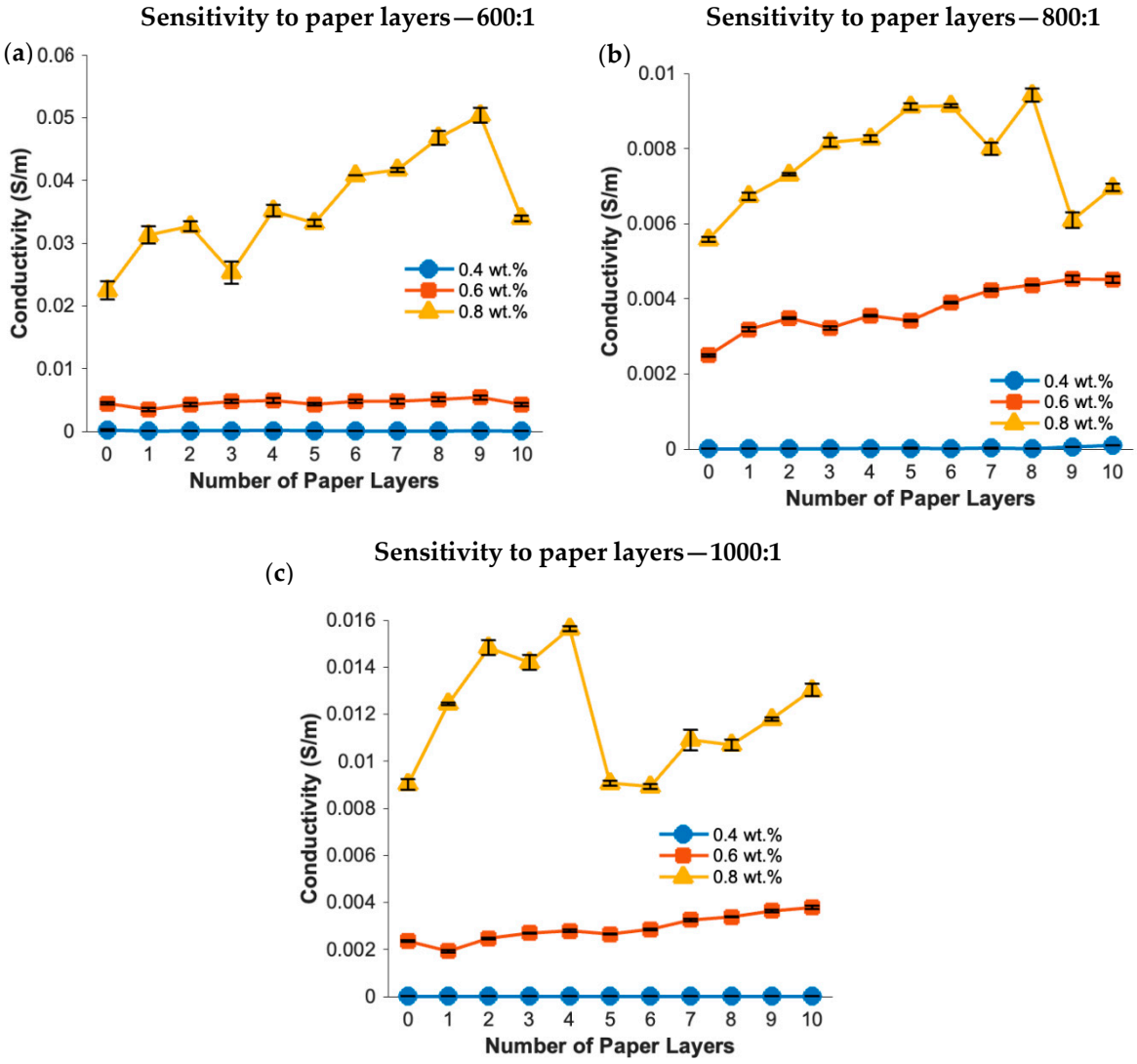


Figure 3. Conductivity of CNT/BBE composites as a function of paper layers applied to the sample surface with CNT loadings of 0.4, 0.6 and 0.8 wt.% for PDMS/CL ratios of (**a**) 600:1, (**b**) 800:1, and (**c**) 1000:1.

For the 600:1 formulation in Figure 3a, the 0.8 wt.% CNT composite exhibited the highest conductivity (>0.02 S/m) with noticeable fluctuations as the number of paper

layers increased. This behavior indicates that dense conductive networks at higher filler loadings experience local compression of CNT junctions under pressure with temporary disruption or reorganization due to uneven stress disruption within the relatively stiff matrix. In contrast the 0.6 wt.% composite displayed significantly lower but more consistent conductivity (~0.005 S/m) across all layers, reflecting a more stable percolation network. The 0.4 wt.% sample showed conductivities below 0.4×10^{-4} S/m but demonstrated distinct spikes at higher loads as seen in Supplementary Figure S9a, likely caused by brief conductive links forming between CNTs when the material is compressed.

At the 800:1 ratio in Figure 3b, the same conductivity hierarch was observed. The 0.8 wt.% samples reached peak conductivities around 0.009 S/m, increasing progressively with additional layers, while the 0.6 wt.% samples exhibited relatively smoother, monotonic increased with a smaller magnitude of change. The linearity of the 0.6 wt.% composite suggest that the softer matrix distributes compressive strain more uniformly, maintaining network connectivity. The 0.4 wt.% sample again displayed low conductivity but a clear upward trend with additional layers as in Supplementary Figure S9b, which is likely due to realignment of the CNTs or compression that enhances conductive contacts [32].

For the 1000:1 composite in Figure 3c, the same overall conductivity trends were observed. The 0.8 wt.% samples maintained high conductivity with oscillations, reflecting a highly compressible yet percolated network. The 0.6 wt.% samples showed very small fluctuations with a stable incremental increase in conductivity with layer count, again confirming its superior stability and repeatability. The 0.4 wt.% sample remained below the percolation threshold, exhibiting irregular peaks at mid-range pressures in Supplementary Figure S9c, possibly due to CNT reorientation.

Overall, these results reinforce the composition-dependent trade-off between absolute conductivity and stability. Higher CNT concentrations enhance conductivity but are prone to instability due to microstructural rearrangements. Alternatively, moderate CNT loadings yield lower conductivity but greater stability under changing pressure.

3.5. Fatigue Performance

Figure 4a–c show the conductivity changes in the BBE/CNT composites under repeated bending cycles up to 1000 cycles for PDMS/CL ratios of 600:1, 800:1, and 1000:1. This test evaluated how well the conductive network withstands cyclic deformation and fatigue.

For the 600:1 formulation in Figure 4a, the 0.8 wt.% CNT composite exhibited the highest conductivity but also the largest fluctuations across the cycles. These oscillations imply repeated deformation and breakage of conductive junction during bending, which is typical of dense CNT networks embedded in relatively stiff matrices [33]. The 0.6 wt.% sample showed a lower but more stable conductivity (~0.004 S/m) throughout the 1000 cycles, indicating a well-balanced network that can deform elastically while maintaining continuous percolation paths. The 0.4 wt.% sample had low conductivity ($< 3 \times 10^{-5}$ S/m) in Supplementary Figure S10a and displayed multiple spikes at early cycles, which is likely due to temporary reconnection of the isolated CNT clusters.

For the 800:1 composite in Figure 4b, the 0.8 wt.% showed a slightly improved stability compared to the 600:1 formulation, where larger oscillations were observed. The reduced fluctuation indicates that the lower crosslinking density provided greater compliance, allowing the network to deform more uniformly without extensive microcracking or localized separation of CNT junctions. However, the 0.6 wt.% sample at this ratio displaced slightly greater variability with spikes in conductivity at 600 and 1000 cycles. This suggests that as the matrix softens, moderate CNT networks may begin to partially reorganize under cyclic strain, leading to local resistive changes. This consequently affects the performance as the bending locations were intentionally changed during the tests to simulate future

real-world applications. The 0.4 wt.% sample again showed very low conductivity as presented in Supplementary Figure S10b with minor intermittent spikes, likely due to temporary reconnection of isolated CNT clusters.

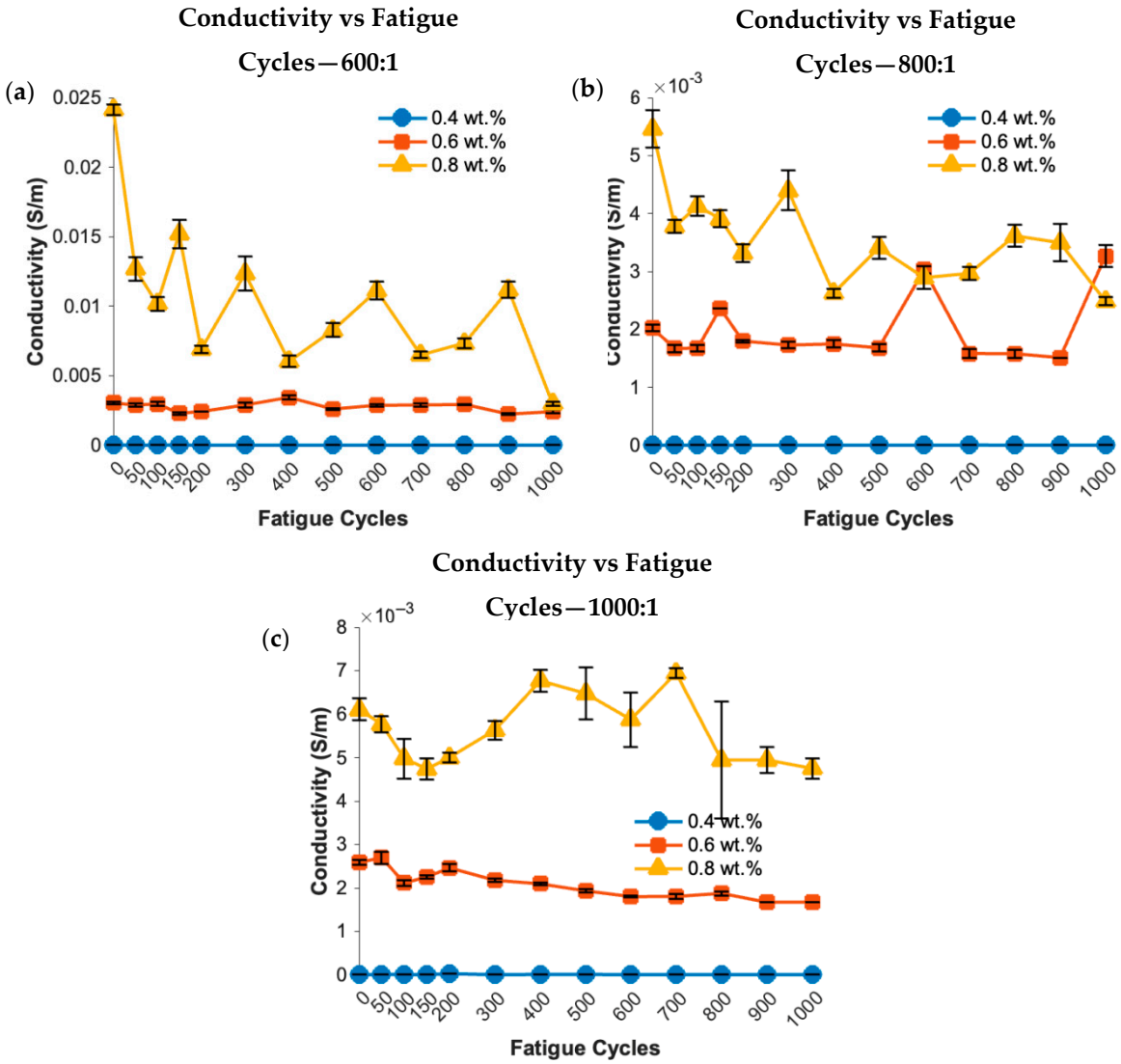


Figure 4. Conductivity of CNT/BBE composites during 1000 cycle manual bending for different CNT loadings of 0.4, 0.6, and 0.8 wt.% and PDMS/CL ratios of (**a**) 600:1, (**b**) 800:1, and (**c**) 1000:1.

For the 1000:1 formulation in Figure 4c, the 0.8 wt.% sample exhibited the highest conductivity but with spikes and drift, reflecting less stable network behavior. This instability likely arises from the highly compliant matrix and extensive CNT interconnectivity, which promotes slippage and recontact between conductive networks during bending. In contrast, the 0.6 wt.% samples maintained relatively consistent conductivity throughout cycling, indicating that moderate CNT loading can better accommodate cyclic strain without causing large-scale disruption of the network. The 0.4 wt.% samples remained below the percolation threshold, showing minimal conductivity and many fluctuations in Supplementary Figure S10c.

Overall, these findings show that the 600:1 formulation offered the highest stability for moderate CNT loadings, while the 800:1 composition improved the stability of the 0.8 wt.% networks by enabling more elastic deformation. However, in the soft matrix (1000:1), both high and moderate CNT loadings experienced decreases in conductivity over cycling. This

confirms that both crosslink density and filler concentration must be optimized to balance conductivity, flexibility, and long-term stability in soft electronic materials.

Additionally, post-fatigue SEM analysis of test samples was performed, such as the 600:1 composite in Supplementary Figure S7, which revealed that the CNT networks remained well dispersed and structurally intact after repeated bending. Although minor surface roughening was observed, no significant cracking was detected.

3.6. Normalized Conductivity Comparison

The normalized conductivity plots (Figures S11–S16) highlight the strain-dependent response of the CNT/BBE composites under bending, pressure, and cyclic loading, comparing measurements obtained with both the two-point probe and four-point methods. Normalization was performed to eliminate the influence of initial conductivity differences among compositions, allowing visual comparison of relative changes in the trend of electrical performance under deformation rather than quantitative evaluation across different samples.

In the two-point probe data, conductivity decreased steadily with the bending angle, particularly for the 0.4 wt.% and 0.6 wt.% sample, indicating disruption of less connected CNT networks. The 0.8 wt.% composites retained higher normalized conductivity due to denser CNTs. Under pressure (Supplementary Figure S12), conductivity increased with applied loads, with the 0.4 wt.% sample showing the steepest rise. Fatigue testing (Supplementary Figure S13) showed a gradual decrease in conductivity for all samples.

The four-point probe method (Figures S14–S16) revealed sharper variation, particularly at low CNT loadings, as contact resistance effects were eliminated. The 0.4 wt.% samples exhibited large fluctuation due to reformation of the CNTs and sparse conductive networks. Compared to the two-point setup, the four-point method captures intrinsic conductivity changes more accurately, suggesting that apparent stability in two-point data may partly arise from probe contact resistance. Overall, the four-point configuration may better reflect true material performance.

4. Discussion

This study demonstrates the significant potential of BBEs/CNTs composites as tunable materials for next-generation soft electronic devices and health monitoring. By systematically varying the PDMS/crosslinker ratio and CNTs loading, we demonstrated how electrical conductivity, mechanical flexibility, pressure sensitivity, and fatigue resistance can be tailored to suit specific application requirements. These results offer a foundation for material optimization across diverse use cases. from wearable sensors to soft robotics.

A key outcome of this work is the trade-off between conductivity and electrical stability. Composites with higher CNT content (0.8 wt.%) exhibited the highest conductivities across all formulations (up to 0.016 S/m for the four-point probe method) at 600:1, but these samples demonstrated greater signal fluctuations during bending and cyclic testing. This variability likely originated from local rearrangement of CNT clusters and intermittent junction breakage within dense percolation networks. Conversely, moderate CNT loading (0.6 wt.%) consistently produced lower but more stable conductivity, as the networks were sufficiently connected to maintain conductivity while allowing elastic deformation of the polymer backbone. These characteristics suggest that the 0.8 wt.% composites are best suited for applications requiring higher conductivity and sensitivity to deformation, such as conductive electrode layers, while the 0.6 wt.% composites offer enhanced reliability and reproducibility for wearable pressure sensors and soft robotic systems where stability is critical. The 0.4 wt.% composites remained below the percolation threshold and showed

weak but detectable responses, indicating potential utility in low-pressure tactile sensing were subtle changes in contact resistance are desirable.

During fatigue testing, the 600:1 formulation exhibited the most stable performance for moderate CNT loading, whereas the 800:1 formulation improved the deformation tolerance of the 0.8 wt.% networks. However, in the highly flexible 1000:1 formulation, high CNT composition increased fluctuation over different cycles, highlighting that excessive matrix softness can compromise network stability. Importantly, bending location was deliberately changed between fatigue cycles to mimic real-world conditions experienced by soft robotic devices. While this approach provides a realistic evaluation of use conditions, it may also have induced local strain variations. Additionally, the current study was limited to manual bending up to 1000 cycles. Automated flexing with controlled amplitude, frequency, and in situ monitoring will be essential for future work to characterize long-term electrical drift, recovery behavior, and potential temperature effects during repeated deformation. Conducting extended cycling tests would provide a more rigorous assessment of network stability and help establish the reliability of BBE/CNT composites for soft electronic applications. Furthermore, this study explored mechanical fatigue and pressure responsiveness, but other environmental factors such as biocompatibility need to be assessed to determine suitability for wearable devices [2]. Finally, this study focused on cyclic bending to assess fatigue performance; future work will need to include uniaxial tensile testing to quantitatively evaluate tensile strength, modulus, and elongation at the break. This will enable a direct comparison between mechanical performance, electrical, and morphological properties.

Future research may also focus on enhancing the directional (anisotropic) conductivity of the composites by aligning CNTs during curing, which may further improve performance in stretchable interconnects or directional sensors. Incorporating hybrid nanofillers, such as silver nanowires, may offer a new strategy to further improve conductivity while tailoring mechanical behavior.

Together, the combination of conductivity, sensitivity, and durability results in this work establishes a design framework for BBEs/CNTs composites. By tuning crosslinking density and CNTs content, materials can be custom designed for their intended function, prioritizing sensitivity, flexibility, or durability as needed. This adaptability underscores the versatility of BBEs/CNTs composites for integration into soft, stretchable, and wearable electronics, paving the way for future innovations in human–machine interfaces, soft prosthetics, and flexible health monitoring devices.

While this study focuses on how variations in material compositions affect the electromechanical behavior of the resulting BBE/CNT composites, Supplementary Table S2 summarizes their performance relative to other reported PDMS-based bottlebrush elastomers [11,29,30]. It is important to note that conductivity in this work was measured using both two-point and four-point probe methods, whereas prior studies employed the two-point approach. Additionally, one set of results is given in Table S2, which exhibits a good balance between conductivity and signal stability as discussed in the Results above. As seen, the two-point results were consistent with previously reported values, confirming alignment with the literature and supporting the use of the composites for benchmarking and application testing, such as ECG signal acquisition and the development of wearable sensors in the future.

5. Conclusions

This study demonstrates the potential to finely tune the electrical and fatigue performance of PDMS-based bottlebrush elastomers via the PDMS/crosslinker ratio and the concentration of single-walled carbon nanotubes (CNTs). The results demonstrate a trade-off between conductivity and stability. Higher CNT content (0.8 wt.%) produced greater

conductivity, whereas moderate loading (0.6 wt.%) yielded more stable and repeatable performance under bending, pressure, and cyclic deformation. The 600:1 formulation offered the best balance between network stability and conductivity, while the 800:1 formulation enhanced the elasticity of the CNT network. In contrast, the 1000:1 composite exhibited increased variability due to excessive matrix softness. These results suggest that CNT/BBE composites can be engineered to prioritize either high conductivity for applications such as electrodes or signal stability for wearable sensors. By optimizing both CNT content and crosslinking density, these materials present a versatile platform for soft electronics, human–machine interfaces, and flexible sensing systems.

Supplementary Materials: The following supporting information can be downloaded at: https://www.mdpi.com/article/10.3390/pr13113613/s1, Figure S1: Schematic of the overall process; Figure S2: In-house purification column to purify PDMS and crosslinker; Figure S3: Reaction mechanism of AIBN-initiated crosslinking of PDMS-based bottlebrush elastomers; Figure S4: (a) Example of the 3D printed wedge (45°) used for angle dependent conductivity testing. (b) Example of the 3D printed wedge (30°) with half the sample was placed on the wedge and the other half placed on the surface with the four-point probe placed at the bending angle; Figure S5: Fatigue testing method. Samples were manually bent over a 90° angle and then returned to flat for repeated cycle counts of 50~1000; Figure S6: Elemental carbon (C-K) count maps of BBE/CNT composites with CNT loadings of (a) 0.4 wt.%, (b) 0.6 wt.%, (c) 0.8 wt.% at PDMS:crosslinker ratio of 600:1; Figure S7: SEM images of the 600:1 BBE/CNT composite after 1000 manual bending cycles, showing a continuous surface morphology and preserved CNT network; Figure S8: Conductivity of 0.4 wt.% CNT/BBE composites under bending angles (0–90°) at PDMS:crosslinker ratios of (a) 600:1, (b) 800:1, and (c) 1000:1; Figure S9: Conductivity response of 0.4 wt.% CNT/BBE composites as a function of paper layers with PDMS:crosslinker ratios of (a) 600:1, (b) 800:1, and (c) 1000:1; Figure S10: Conductivity response of 0.4 wt.% CNT/BBE composites measured over 1000 bending cycles at PDMS:crosslinker ratios of (a) 600:1, (b) 800:1, and (c) 1000:1; Figure S11: (a) Conductivity vs PDMS:crosslinker (CL) ratio (600:1, 800:1, 1000:1) at 0.4, 0.6, and 0.8 CNT wt%. (b–d) Normalized conductivity to 0° of 600:1 (b), 800:1 (c), and 1000:1 (d) samples with 0.4, 0.6, and 0.8 CNTs wt% at bending angles of 15°, 30°, 45°, 60°, 75°, 90° using the two-point probe method; Figure S12: (a–c) Normalized conductivity for the sensitivity of 0–10 paper layers for each BBE:CL ratio (600:1, 800:1, 1000:1) and CNT wt% (0.4, 0.6, 0.8 wt%) using the two-point probe method; Figure S13: (a–c) Normalized conductivity of BBEs/CNTs composites over multiple fatigue cycles. Samples were tested at intervals of 100, 200, 300 cycles under repeated mechanical deformation using the two-point probe method; Figure S14: (a–c) Normalized conductivity of CNT/BBE composites measured by the four-point probe under bending using the four-point probe at PDMS:CL ratios of 600:1, 800:1, and 1000:1, respectively with CNT loadings of 0.4, 0.6 and 0.8 wt.%; Figure S15. (a–c) Normalized conductivity response of CNT/BBE composites under incremental pressure (0-1 0 paper layers) using the four-point probe for PDMS:CL ratios of 600:1, 800:1, and 1000:1 respectively with CNT loadings of 0.4, 0.6 and 0.8 wt.%; Figure S16. (a–c) Normalized conductivity of CNT/BBE composites over 0–1000 fatigue cycles using the four-point probe; Table S1: Formulations for each PDMS, crosslinker and AIBN mixtures with different CNT loadings; Table S2: Comparison of electrical and mechanical performance of this work with previously reported CNT/PDMS-based and bottlebrush elastomer conductors.

Author Contributions: Y.D.: conceptualization, investigation, manuscript writing and reviewing, project supervision, and funding acquisition. A.J.: investigation, results interpretation and visualization, and manuscript writing. All authors have read and agreed to the published version of the manuscript.

Funding: This research was funded by the National Science Foundation, grant numbers 2143268 and 2426614.

Data Availability Statement: The original contributions presented in this study are included in the article/Supplementary Materials. Further inquiries can be directed to the corresponding author.

Acknowledgments: The authors acknowledge financial support from the National Science Foundation. During the preparation of this manuscript, the authors used Canva AI (Canva, 2025) to generate and refine three schematic figures (Figures S1, S2 and S5).

Conflicts of Interest: The authors declare no conflicts of interest. The funders had no role in the design of the study; in the collection, analyses, or interpretation of data; in the writing of the manuscript; or in the decision to publish the results.

References

1. Yang, M.; Peng, K.; Li, Z.; Gao, Y.; Tian, Q.; Zhou, Z.; Chen, Y. Recent progress in flexible materials for wearable devices for body function and athletic performance monitoring. *Chem. Eng. J.* **2025**, *505*, 159659. [CrossRef]
2. Amjadi, M.; Kyung, K.-U.; Park, I.; Sitti, M. Stretchable, skin-mountable, and wearable strain sensors and their potential applications: A Review. *Adv. Funct. Mater.* **2016**, *26*, 1678–1698. [CrossRef]
3. Kim, H.; Watkins, J.J.; Crosby, A.J. Adhesion and mechanical properties of poly(dimethylsiloxane) bottlebrush elastomers. *Soft Matter* **2023**, *19*, 5311–5317. [CrossRef] [PubMed]
4. Yuan, Y.; Liu, B.; Li, H.; Li, M.; Song, Y.; Wang, R.; Wang, T.; Zhang, H. Flexible Wearable Sensors in Medical Monitoring. *Biosensors* **2022**, *12*, 1069. [CrossRef]
5. Miranda, I.; Souza, A.; Sousa, P.; Ribeiro, J.; Castanheira, E.M.; Lima, R.; Minas, G. Properties and applications of PDMS for Biomedical Engineering: A Review. *J. Funct. Biomater.* **2021**, *13*, 2. [CrossRef]
6. Li, S.; Zhang, J.; He, J.; Liu, W.; Wang, Y.; Huang, Z.; Pang, H.; Chen, Y. Functional PDMS Elastomers: Bulk Composites, Surface Engineering, and Precision Fabrication. *Adv. Sci.* **2023**, *10*, e2304506. [CrossRef]
7. Self, J.L.; Reynolds, V.G.; Blankenship, J.; Mee, E.; Guo, J.; Albanese, K.; Xie, R.; Hawker, C.J.; de Alaniz, J.R.; Chabinyc, M.L.; et al. Carbon Nanotube Composites with Bottlebrush Elastomers for Compliant Electrodes. *ACS Polym. Au* **2021**, *2*, 27–34. [CrossRef]
8. Boland, C.S.; Khan, U.; Ryan, G.; Barwich, S.; Charifou, R.; Harvey, A.; Backes, C.; Li, Z.; Ferreira, M.S.; Coleman, J.N. Sensitive electromechanical sensors using viscoelastic graphene-polymer nanocomposites. *Composites* **2016**, *354*, 1257–1260. [CrossRef]
9. Kim, T.G.; Eom, H.S.; Kim, J.H.; Jung, J.K.; Jang, K.-S.; Lee, S.J. Electrically Conductive Silicone-Based Nanocomposites. *ACS Omega* **2021**, *6*, 31876–31890. [CrossRef]
10. Le, M.L.; Lapkriengkri, I.; Albanese, K.R.; Nguyen, P.H.; Tran, C.; Blankenship, J.R.; Segalman, R.A.; Bates, M.M.; Chabinyc, M.L. Engineering Soft, Elastic, and Conductive Polymers for Stretchable Electronics Using Ionic Compatibilization. *Chem. Mater.* **2023**, *35*, 7301–7310. [CrossRef]
11. Xu, P.; Wang, S.; Lin, A.; Min, H.-K.; Zhou, Z.; Dou, W.; Sun, Y.; Huang, X.; Tran, H.; Liu, X. Conductive and elastic bottlebrush elastomers for Ultrasoft Electronics. *Nat. Commun.* **2023**, *14*, 623. [CrossRef] [PubMed]
12. Jin, C.; Wang, Z.; Volinksky, A.A.; Sharfeddin, A.; Gallant, N.D. Mechanical characterization of crosslinking effect in polydimethylsiloxane using nanoindentation. *Polym. Test.* **2016**, *56*, 329–336. [CrossRef]
13. Andrews, R.; Weisenberger, M.C. Carbon nanotube polymer composites. *Curr. Opin. Solid State Mater. Sci.* **2004**, *8*, 31–37. [CrossRef]
14. Peng, S.; Yu, Y.; Wu, S.; Wang, C.-H. Conductive polymer nanocomposites for stetchable electronics: Material selection, design, and applications. *ACS Appl. Mater. Interfaces* **2021**, *13*, 43831–43854. [CrossRef]
15. Adu, P.C.O.; Aakyiir, M.; Su, X.; Alam, J.; Tran, L.C.; Dai, J.; Meng, Q.; Kuan, H.-C.; Ma, J. Challenges and advancements in elastomer/CNT nanocomposites with mechanochemical treatment, reinforcement mechanisms and applications. *Smart Mater. Manuf.* **2024**, *2*, 100053. [CrossRef]
16. Adeli, Y.; Venkatesan, T.R.; Nuesch, F.A.; Opris, D.M. Elastomers based on polynorbornene with polar polysiloxane brushes for soft transducer applications. *Helvetica Chim. Acta* **2024**, *107*, e202400032. [CrossRef]
17. Bulut, M.S.; Ordu, M.; Der, O.; Basar, G. Sustainable thermoplastic material selection for hybrid vehicle battery packs in the automotive industry: A comparative multi-criteria decision making approach. *Polymers* **2024**, *16*, 2768. [CrossRef]
18. Maaskant, E.; Post, W.; Brouwer, M.T.; van Es, D.S.; van Velzen, E.T. Strategic selection tool for thermoplastic materials in a renewable circular economy: Identifying future circular polymers. *Sustain. Prod. Consum.* **2023**, *38*, 174–185. [CrossRef]
19. Asadi, V.; Dolleman, R.; van der Gucht, J.; Kodger, T.E. 3D printable soft and solvent-free thermoplastic elastomers containing dangling bottlebrush chains. *Mater. Adv.* **2023**, *4*, 5535–5545. [CrossRef] [PubMed]
20. Debriabin, K.V.; Dobrynin, M.V.; Islamova, R.M. A metal-free radical technique for cross-linking of polymethylhydrosiloxane or polymethylvinylsiloxane using AIBN. *Dalton Trans.* **2020**, *49*, 8855–8858. [CrossRef]
21. Clarke, B.R.; Kim, H.; Ilton, M.; Watkins, J.J.; Crosby, A.J.; Tew, G.N. The impact of polymerization chemistry on the mechanical properties of poly(dimethylsiloxane) bottlebrush elastomers. *Macromolecules* **2022**, *55*, 10312–10319. [CrossRef]
22. Esteves, A.; Brokken-Zijp, J.; Laven, J.; Huinink, H.; Reuvers, N.; Van, M.; de With, G. Influence of cross-linker concentration on the cross-linking of PDMS and the network structures formed. *Polymer* **2009**, *50*, 3955–3966. [CrossRef]

23. Marlow, M.; Wehrstedt, K.-D.; Manolov, M. Thermal decomposition of AIBN Part A: Decomposition in real scale packages and SADT determination. *Thermochim. Acta* **2015**, *621*, 1–5. [CrossRef]
24. Birch, M.E.; Ruda-Eberenz, T.A.; Chai, M.; Andrrews, R.; Hatfield, R.L. Properties that influence the specific surface areas of carbon nanotubes and nanofibers. *Ann. Occup. Hyg.* **2013**, *57*, 1148–1166.
25. Huang, Y.Y.; Terentjev, E.M. Dispersion of carbon nanotubes: Mixing, sonication, stabilization, and composite properties. *Polymers* **2012**, *4*, 275–295. [CrossRef]
26. Ma, P.-C.; Siddiqui, N.A.; Marom, G.; Kim, J.-K. Dispersion and functionalization of carbon nanotubes for polymer-based nanocomposites: A review. *Compos. Part A Appl. Sci. Manuf.* **2010**, *41*, 1345–1367. [CrossRef]
27. Romero, G.; Wang, X. Chemistry LibreTexts. LibreTexts. 30 June 2023. Available online: https://chem.libretexts.org/Bookshelves/Inorganic_Chemistry/Supplemental_Modules_and_Websites_(Inorganic_Chemistry)/Catalysis/Catalyst_Examples/Hydrosilylation (accessed on 21 October 2025).
28. Lienemann, S.; Boda, U.; Mohammadi, M.; Zhou, T.; Petsagkourakis, I.; Kim, N.; Tybrandt, K. Exploring the elastomer influence on the electromechanical performance of stretchable conductors. *ACS Appl. Mater. Interfaces* **2024**, *16*, 38365–38376. [CrossRef] [PubMed]
29. Shao, J.; Yu, L.; Skov, A.L.; Daugaard, A. Highly stretchable conductive MWCNT-PDMS composite with self-enhanced conductivity. *J. Mater. Chem. C* **2020**, *8*, 13389–13395. [CrossRef]
30. Zeng, J.; Ma, W.; Wang, Q.; Yu, S.; Innocent, M.T.; Xiang, H.; Zhu, M. Strong, high stretchable and ultrasensitive SEBS/CNTs hybrid fiber for high-performance strain sensor. *Compos. Commun.* **2021**, *25*, 100735. [CrossRef]
31. Wu, D.; Wei, M.; Li, R.; Xiao, T.; Gong, S.; Xiao, Z.; Zhu, Z.; Li, Z. A percolation network model to predict the electrical property of flexible CNT/PDMS composite films fabricated by spin coating technique. *Compos. Part B Eng.* **2019**, *174*, 107034. [CrossRef]
32. Kim, H.; Hong, S.-K.; Ryu, J.-K.; Park, S.-H. Effect of filler alignment on piezo-resistive and mechanical properties of carbon nanotube composites. *Materials* **2020**, *13*, 2598. [CrossRef] [PubMed]
33. Kanoun, O.; Bouhamed, A.; Ramalingame, R.; Bautista-Quijano, J.; Rahebdrab, D.; Al-Hamry, A. Review on conductive polymer/CNTs nanocomposites based flexible and stretchable strain and pressure sensors. *Sensors* **2021**, *21*, 341. [CrossRef] [PubMed]
34. Bauhofer, W.; Kovacs, J.Z. A review and analysis of electrical percolation in carbon nanotube polymer composites. *Compos. Sci. Technol.* **2009**, *69*, 1486–1498. [CrossRef]
35. Eisape, A.; Rennoll, V.; Van Volkenburg, T.; Xia, Z.; West, J.E.; Kang, S.H. Soft CNT-polymer composites for high pressure sensors. *Sensors* **2022**, *22*, 5268. [CrossRef] [PubMed]

Disclaimer/Publisher's Note: The statements, opinions and data contained in all publications are solely those of the individual author(s) and contributor(s) and not of MDPI and/or the editor(s). MDPI and/or the editor(s) disclaim responsibility for any injury to people or property resulting from any ideas, methods, instructions or products referred to in the content.